Check for updates

NITROGEN CYCLE

Natural $^{15}N^{15}N$ abundances constrain fixed nitrogen loss

Jiarui Liu[1,2]*, David L. Valentine[1,3]*, Annie Bourbonnais[4], Dale T. Andersen[5], Daniele Bianchi[6], Grace Brown[7,8], M. Bayani Cardenas[9], Daniel Fillion[10], Claudia Frey[11], Kelsey M. Gosselin[12], Aoshuang Ji[13], Franklin S. Kinnaman[1,3], Denis Lacelle[14], Moritz F. Lehmann[11], Katelyn McPaul[7,8], James Mullahoo[15], Victoria J. Orphan[15,16], André Pellerin[10], Elen Reji[4], Elizabeth D. Swanner[17], Tina Treude[2], Alan M. Seltzer[8,18], Edward D. Young[2]*

Nitrogen regulates primary productivity across much of the biosphere, yet fixed nitrogen loss remains poorly constrained because existing methods rely on indirect proxies or ex situ experiments. In this study, we show that natural abundances of the rare $^{15}N^{15}N$ isotopologue of dinitrogen (N_2) provide a direct tracer of biological N_2 production across diverse aquatic environments. N_2 produced by denitrification and anammox has a near-stochastic $^{15}N^{15}N$ distribution [0 per mil (‰)], whereas atmospheric N_2 carries a distinct $^{15}N^{15}N$ excess (19‰), allowing the two sources to be quantitatively distinguished. Across aquifers, stratified lakes, coastal basins, oxygen minimum zones, and marine sediments, $^{15}N^{15}N$ measurements reveal widespread nitrogen loss previously obscured by physical gas accumulation and nitrogen fixation. Natural $^{15}N^{15}N$ abundances therefore provide a general framework for directly constraining fixed nitrogen loss across the aquatic nitrogen cycle.

Nitrogen (N) is an essential component of life, and the balance between its sources and sinks in aquatic environments regulates ecosystem productivity, water quality, and the long-term stability of the global fixed N inventory. Microbial conversion of fixed N to inert dinitrogen (N_2) through denitrification and anaerobic ammonium oxidation (anammox) returns biologically available nitrogen to the atmosphere, closing the global nitrogen cycle (*1*, *2*). Yet the magnitude of fixed N loss remains one of the greatest uncertainties in Earth's major biogeochemical cycles (*3*–*7*).

Despite decades of study, quantifying fixed N loss in natural environments remains difficult (*8*, *9*). Global budgets are typically inferred indirectly from stoichiometric and mass balance approaches, excess N_2 estimates based on N_2/Ar ratios, and extrapolated rates from incubation experiments (*10*–*13*). These methods either integrate signals over large spatial and temporal scales, requiring assumptions about background conditions and transport, or depend on ex situ rate measurements that represent only ephemeral conditions. Stoichiometric approaches such as *N** depend on assumed N:P relationships that vary in space and time and remain poorly constrained (*10*, *14*), whereas mass balance and inverse models infer fixed N loss indirectly from budget residuals or nutrient distributions and are therefore sensitive to flux constraints and model assumptions, introducing substantial uncertainty into globally integrated rates (*9*, *13*, *15*). N_2/Ar ratios are sensitive to air-water gas exchange, dissolution of entrained air bubbles, and temperature-dependent solubility; because Ar is approximately twice as soluble as N_2, these processes can shift N_2/Ar independently of biological N_2 production (*16*–*18*). Incubation experiments using ^{15}N-labeled tracer or inhibitors may perturb microbial activity, alter in situ rates, and provide only snapshots that may not be representative at broader spatiotemporal scales (*8*, *12*). Together, these limitations underscore the need for a direct tracer of biological N_2 production independent of physical gas exchange and experimental manipulation.

We use the natural abundance of the rare $^{15}N^{15}N$ isotopologue of N_2 as a direct and sensitive tracer of fixed N loss. The parameter Δ_{30}, which quantifies the deviation in $^{15}N^{15}N$ abundance from that expected for a random distribution of nitrogen isotopes among N_2 molecules, is defined as $\Delta_{30} = {}^{30}R/({}^{15}R)^2 - 1$ (‰), where ${}^{30}R = {}^{15}N^{15}N/{}^{14}N^{14}N$ and ${}^{15}R = {}^{15}N/{}^{14}N$ for the gas of interest. Atmospheric N_2 exhibits a well-defined Δ_{30} of 19.1 per mil (‰) ($\Delta_{30,atm}$), an enrichment interpreted to originate from upper-atmospheric nitrogen chemistry, where energetic solar radiation and charged particles dissociate and reform N_2 (*19*). Isotopologue-specific effects during these bond-breaking and bond-forming reactions are thought to enrich the rare $^{15}N^{15}N$ isotopologue, generating the high-Δ_{30} anomaly observed in atmospheric N_2. Conversely, N_2 produced by microbial denitrification and anammox ($\Delta_{30,bio}$) exhibits a near-stochastic isotopologue distribution, in which ^{14}N and ^{15}N atoms are paired randomly during N_2 formation (*19*, *20*). In the stochastic endmember, the relative abundance of $^{15}N^{15}N$ scales with the square of the bulk $^{15}N/^{14}N$ ratio, and Δ_{30} is therefore 0‰. Nitrogen fixation does not measurably alter Δ_{30} (*19*). Mixing between atmospheric and biogenic N_2 therefore produces a predictable decrease in Δ_{30} that directly records the fraction of biogenic N_2 (f_{bio}) in a sample (Eq. 1) (*20*, *21*).

$$\Delta_{30,sample} = (1 - f_{bio})\Delta_{30,atm} + f_{bio}\Delta_{30,bio} \quad (1)$$

Unlike tracers such as N_2/Ar, Δ_{30} reflects molecular origin rather than N_2 accumulation, making it insensitive to the direct effects of gas exchange, temperature change, or addition of air bubbles. Although air-water gas exchange can shift the measured Δ_{30} value through mixing with atmospheric N_2, it does not fractionate Δ_{30} and instead transports the existing biological signal. Thus, natural $^{15}N^{15}N$ abundances provide a source-specific tracer of biologically produced N_2. Below, we apply high-precision Δ_{30} measurements to a diverse range of aquatic environments—spanning nitrate-rich groundwater, stratified lakes, coastal hypoxic basins, open-ocean oxygen minimum zones, and marine sediments—to demonstrate that natural $^{15}N^{15}N$ abundances can constrain fixed N loss without relying on the corrections and assumptions required by conventional gas- and nutrient-based approaches.

Resolving groundwater denitrification independent of excess air

Groundwater denitrification is commonly evaluated by using dissolved N_2/Ar ratios (*22*, *23*), in which Ar serves as a proxy for the atmospheric component of dissolved N_2 inherited from air-water equilibrium. However, fluctuations in the water table can trap air bubbles that dissolve into groundwater, producing excess air and gas supersaturation that are ubiquitous in aquifers worldwide (*24*). Because N_2 and Ar differ in solubility, this process alters N_2/Ar ratios and complicates identification of biogenic N_2. In principle, excess air can be constrained using additional noble gases (e.g., Ne, Ar, Kr, Xe) through inverse modeling (*25*). In practice,

[1]Marine Science Institute, University of California, Santa Barbara, Santa Barbara, CA, USA. [2]Department of Earth, Planetary, and Space Sciences, University of California, Los Angeles, Los Angeles, CA, USA. [3]Department of Earth Science, University of California, Santa Barbara, Santa Barbara, CA, USA. [4]School of the Earth, Ocean and Environment, University of South Carolina, Columbia, SC, USA. [5]Carl Sagan Center, SETI Institute, Mountain View, CA, USA. [6]Department of Atmospheric and Oceanic Sciences, University of California, Los Angeles, Los Angeles, CA, USA. [7]MIT-WHOI Joint Program in Oceanography/Applied Ocean Science and Engineering, Cambridge and Woods Hole, MA, USA. [8]Marine Chemistry and Geochemistry Department, Woods Hole Oceanographic Institution, Woods Hole, MA, USA. [9]Department of Earth and Planetary Sciences, University of Texas at Austin, Austin, TX, USA. [10]Institut des Sciences de la Mer, Université du Québec à Rimouski, Rimouski, Québec, Canada. [11]Department of Environmental Sciences, University of Basel, Basel, Switzerland. [12]Interdepartmental Graduate Program in Marine Science, University of California, Santa Barbara, Santa Barbara, CA, USA. [13]Department of Earth and Planetary Sciences, University of California, Riverside, Riverside, CA, USA. [14]Department of Geography, Environment and Geomatics, University of Ottawa, Ottawa, Ontario, Canada. [15]Division of Geological and Planetary Sciences, California Institute of Technology, Pasadena, CA, USA. [16]Division of Biology and Biological Engineering, California Institute of Technology, Pasadena, CA, USA. [17]Department of the Earth, Atmosphere, and Climate, Iowa State University, Ames, IA, USA. [18]School of Earth Sciences, University College Dublin, Dublin, Ireland. ***Corresponding author. Email: jiaruiliu@ucla.edu (J.L.); valentine@ucsb.edu (D.L.V.); eyoung@epss.ucla.edu (E.D.Y.)**

Downloaded from https://www.science.org at University of California Los Angeles on October 08, 2026

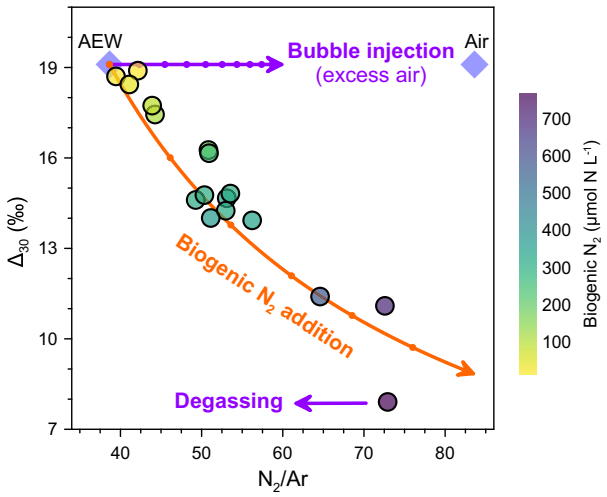


Fig. 1. Constraints on biogenic N_2 in groundwater using Δ_{30} and dissolved gas ratios. Relationship between Δ_{30} and N_2/Ar ratios for groundwater samples from an industrial facility in central Texas. Air-equilibrated water (AEW) defines the initial composition. Dissolution of trapped air bubbles (excess air) increases N_2/Ar with no change in Δ_{30} (purple), whereas addition of biogenic N_2 decreases Δ_{30} while increasing N_2/Ar (orange). Biogenic N_2 concentrations are calculated from Δ_{30} by mass balance between atmospheric and biologically produced N_2. Dots along the modeled trajectories indicate addition of N_2 in increments of 200 µmol N $liter^{-1}$ to the initial dissolved gas pool, supplied either as biogenic N_2 or through atmospheric-air addition. Error bars are smaller than symbols.

however, very few studies use the multiple noble-gas measurements required for modeling (*26*), and nearly all estimates of groundwater biogenic N_2 rely solely on N_2/Ar ratios. Consequently, interpretation of groundwater denitrification hinges on assumptions about the mechanism and magnitude of excess-air dissolution, leading to large systematic uncertainty.

Natural $^{15}N^{15}N$ abundances can resolve these uncertainties. We analyzed groundwater samples from monitoring wells in a nitrate-rich aquifer in central Texas (fig. S1) and found Δ_{30} values ranging from 7.9 to 18.9‰, corresponding to biogenic N_2 concentrations of 12 to 768 µmol N $liter^{-1}$ (Fig. 1). The lowest Δ_{30} value (7.9‰) indicates that 59% of dissolved N_2 was derived from microbial fixed N loss (Eq. 1), providing direct evidence of substantial biological N_2 production within the aquifer.

Biogenic N_2 concentrations derived from Δ_{30} and those inferred from N_2/Ar ratios agree to first order (Fig. 1). In the absence of gas-exchange processes that alter N_2/Ar, all data points in a Δ_{30} versus N_2/Ar plot should lie along the biogenic addition trajectory (orange curve). However, despite this overall agreement, several samples deviate substantially from this trend. Dissolution of trapped air bubbles increases N_2/Ar by introducing air with a higher N_2/Ar ratio than that of dissolved gases at solubility equilibrium (*24*), whereas degassing decreases N_2/Ar through preferential loss of N_2 relative to Ar (*27*). Because Δ_{30} tracks the molecular origin of N_2, scatter away from the orange curve reflects physical overprinting of N_2/Ar rather than ambiguity in the Δ_{30}-based estimate of biogenic N_2.

Natural $^{15}N^{15}N$ abundances therefore provide a source-specific tracer of groundwater fixed N loss without assumptions about excess air or gas equilibration. Replicate analyses yielded a Δ_{30} reproducibility of <0.1‰, equivalent to <0.5% of dissolved N_2 derived from microbial fixed N loss. This high sensitivity allows detection of relatively small biogenic N_2 signals that are difficult to resolve with conventional N_2/Ar-based approaches. This capability has direct implications for groundwater management and remediation monitoring, in which distinguishing biological nitrogen removal from physical gas processes remains a central challenge.

Constraining fixed nitrogen loss in stratified lakes

Stratified lakes provide a natural setting for testing Δ_{30} to quantify biological nitrogen loss under conditions where dissolved-gas inventories are strongly modified by physical processes. In permanently ice-covered Lake Untersee in Antarctica, dissolved gases are supersaturated because freezing at the base of the ice cover rejects gases into the underlying water, while the perennial ice cover suppresses gas exchange and prevents degassing (*28*). Under these conditions, N_2/Ar ratios exceed equilibrium values even at oxic, shallower depths where fixed N loss is absent (figs. S2 and S3).

Despite this gas enrichment, Δ_{30} decreases systematically from the atmospheric value of 19.1 to ~18.7‰ across the permanent oxycline in the southern basin of the lake (Fig. 2A). This decline indicates the accumulation of biologically produced N_2 in the anoxic region of the basin. By deriving the concentration of biogenic N_2 from Δ_{30}, converting its vertical gradient into a turbulent diffusive flux using a vertical eddy diffusivity (K_z) of ~0.004 cm^2 s^{-1} (see supplementary materials), and equating this flux to an areal rate of fixed N loss under a steady-state vertical balance between in situ N_2 production and upward diffusive transport, we estimate a fixed N loss rate of ~0.12 mmol m^{-2} day^{-1}. Although uncertainty in K_z remains difficult to quantify rigorously, the combined Δ_{30} and transport analysis provides a first-order basin-scale constraint on fixed N loss based on a biogenic N_2 gradient that conventional N_2/Ar measurements cannot readily resolve.

Measurements in temperate lakes in Minnesota further illustrate how Δ_{30} isolates gross biological N_2 production despite physical overprinting and concurrent nitrogen fixation. A recent study reported widespread N_2 supersaturation in Upper Midwest lakes on the basis of N_2/Ar measurements and attributed it to denitrification and/or anammox (*29*). However, supersaturation was also observed in oxygenated surface waters, where microbial fixed N loss should be suppressed (*29*). In such settings, elevated N_2/Ar ratios may arise from temperature-driven changes in gas solubility or air-bubble injection during wind-driven turbulence (*30*).

By contrast, Δ_{30} is not affected by these physical processes. Brownie Lake, a lake influenced by anthropogenic nutrient inputs, exhibits a pronounced decrease in Δ_{30} to ~18.4‰ at the oxycline, corresponding to substantial accumulation of biogenic N_2 (Fig. 2B). By contrast, Δ_{30} decreases only slightly to ~18.9‰ in Deming Lake, a forested lake less influenced by nutrient inputs, indicating lower biological N_2 production and fixed N loss (Fig. 2C). The stronger Δ_{30} shift in Brownie Lake reflects elevated anthropogenic nitrogen inputs that support primary productivity above the oxycline and enhance denitrification and/or anammox, with rates estimated at ~2.0 mmol m^{-2} day^{-1} from reactive transport modeling (fig. S4; see supplementary materials). By comparison, primary productivity in Deming Lake is likely nitrogen and phosphorus colimited (*31*) and concentrated near the oxycline, as indicated by chlorophyll a distributions (fig. S5). There, productivity is primarily sustained by ammonium from deeper waters, most of which is recycled within the system rather than converted to N_2, with modeled fixed N loss rates of ~0.2 mmol m^{-2} day^{-1}.

Notably, N_2/Ar ratios in Deming Lake fall below atmospheric equilibrium values, consistent with a net N_2 sink driven by active N_2 fixation (fig. S5) (*31*). This interpretation is supported by previous work showing that Deming Lake is dominated by cyanobacteria and that fixed N availability is low in the oxygenated upper water column, where active N_2 fixation has been demonstrated by $^{15}N_2$-labeling experiments in both the epilimnion and the subsurface oxygen-maximum layer (*31*). Because N_2 fixation does not measurably alter Δ_{30} (*19*), Δ_{30} records the accumulation of biogenic N_2 from gross fixed N loss, independent of concurrent fractional consumption of the N_2 pool by fixation, whereas N_2/Ar reflects the net balance between these opposing fluxes. Together, our measurements in these lakes demonstrate that Δ_{30} provides a robust tracer of biological N_2 production despite N_2 fixation and confounding physical gas processes that modify dissolved-gas inventories.

Downloaded from https://www.science.org at University of California Los Angeles on October 08, 2026

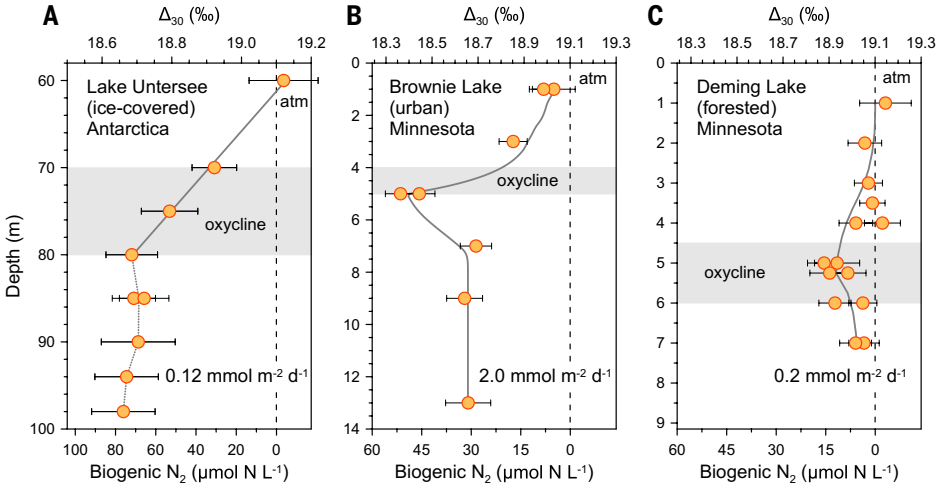


Fig. 2. Vertical distributions of Δ_{30} and biogenic N_2 in stratified lakes. Depth profiles of Δ_{30} and biogenic N_2 concentrations derived from Δ_{30} in three stratified lakes: (**A**) Lake Untersee, (**B**) Brownie Lake, and (**C**) Deming Lake. The dashed vertical line labeled "atm" indicates the atmospheric Δ_{30} value (19.1‰), and the shaded band marks the oxycline. Error bars indicate 1 standard error. The gray line represents a linear regression fit to the biogenic N_2 profile in Lake Untersee and the best-fit reactive transport model results for Brownie and Deming Lakes. Corresponding areal fixed N loss rates are shown in each panel.

The three lakes also show a gradient in how efficiently upward nutrient supply is converted to N_2. Upward ammonium fluxes are ~0.13, 4.8, and 5.5 mmol m^{-2} day^{-1} in Lake Untersee, Brownie Lake, and Deming Lake, respectively (figs. S3 to S5), whereas corresponding Δ_{30}-derived fixed N loss rates are ~0.12, 2.0, and 0.2 mmol m^{-2} day^{-1}. This comparison suggests that most of the upward ammonium supply is converted to N_2 in Lake Untersee, a substantial fraction in Brownie Lake, and only a small fraction in Deming Lake. The offset between ammonium supply and Δ_{30}-derived N_2 production therefore constrains how much regenerated nitrogen is retained within the water column, highlighting the utility of Δ_{30} for assessing nitrogen removal during eutrophication.

Reconciling nutrient and gas proxies of marine nitrogen loss

Using our Δ_{30} measurements in the hypoxic Santa Barbara Basin, we compared Δ_{30}-derived estimates of fixed N loss against N^* and excess N_2 on the basis of N_2/Ar ratios. During spring ventilation events, oxygenated water enters the basin and then becomes progressively depleted in oxygen through microbial respiration (*32*). As oxygen declines through summer and fall, Δ_{30} decreases and biogenic N_2 accumulates (Fig. 3).

In spring 2025, biogenic N_2 concentrations inferred from Δ_{30}, N_2/Ar, and N^* were similar to first order (Fig. 3A). By summer and fall 2025, however, N^* predicts larger fixed N deficits than Δ_{30}-derived biogenic N_2 at greater depths by roughly 20 to 30% (Fig. 3, B and C). This mismatch likely reflects deviations from the assumed Redfield N:P stoichiometry, benthic phosphate release during iron-oxyhydroxide reduction, and/or nitrate storage by sulfide-oxidizing bacteria, which alter nutrient ratios without directly producing N_2 (*33*, *34*). Such bias in N^* would imply corresponding overestimates of fixed N loss, with important implications for marine productivity and nutrient cycling. Interpretation of N_2/Ar is also complicated by corrections for background oceanic N_2 supersaturation, which introduce uncertainties that are difficult to quantify (*17*, *35*). By contrast, Δ_{30} directly records the fraction of biologically produced N_2 in the dissolved N_2 pool without requiring physical corrections.

Vertical gradients in Δ_{30}-derived biogenic N_2 were converted to upward diffusive fluxes by using vertical eddy diffusivity estimates (3.4 ± 1.0 cm^2 s^{-1}) (*36*), yielding fixed N loss rates of 4.9 to 6.1 mmol m^{-2} day^{-1} across individual sampling periods in the Santa Barbara Basin. Accounting for both diffusive export and temporal accumulation of biogenic N_2 within the basin produces integrated rates of 8.7 ± 3.0 mmol m^{-2} day^{-1} from April to August and 13.6 ± 2.8 mmol m^{-2} day^{-1} from August to November (see supplementary materials). These integrated Δ_{30}-based rates represent total N_2 production in the bottom-water layer and thus include both sedimentary and water column denitrification and anammox. Independent constraints from $\delta^{15}N$ of nitrate in bottom waters indicate that 11 to 49% of nitrate loss occurs in the water column (figs. S6 to S9), suggesting that although sedimentary denitrification dominates, water column denitrification is also significant in the Santa Barbara Basin, particularly under anoxic conditions (*37*). In the nearby San Pedro Basin, $\delta^{15}N$ of water column nitrate indicates that denitrification occurs almost exclusively in the sediments, yet the resulting biogenic N_2 accumulates in bottom waters and is captured by Δ_{30} (figs. S10 and S11), demonstrating that bottom-water Δ_{30} integrates sedimentary fixed N loss even where water column denitrification is minimal.

Overall, when interpreted within appropriate transport constraints, Δ_{30} quantifies the absolute magnitude of fixed N loss at the water mass–to-ecosystem scale by integrating N_2 production from both denitrification and anammox, whereas incubation experiments resolve short-term rates and pathway partitioning between denitrification and anammox (*38*), and $\delta^{15}N$ of nitrate constrains the relative contributions of water column versus sedimentary denitrification rather than total N_2 production (*37*). Thus, Δ_{30} offers a long-sought tracer capable of directly quantifying integrated fixed N loss in natural systems.

Oxygen minimum zones (OMZs) are major sites of oceanic water column nitrogen loss (*39*). However, fixed N loss can be difficult to quantify in weak OMZs such as the Bay of Bengal OMZ, where O_2 declines to submicromolar levels but rarely reaches complete anoxia (*40*). Earlier studies found no clear evidence for fixed N loss on the basis of stoichiometric indicators (*41*), whereas more recent work suggested modest loss in the Bay of Bengal (*40*). Uncertainty remains because at these low levels, nutrient-deficit and N_2/Ar-based approaches have limited sensitivity and depend on assumed stoichiometric and background conditions.

Across the core of the Bay of Bengal OMZ, Δ_{30} indicates relatively uniform biogenic N_2 concentrations of ~9.2 ± 2.8 μmol N $liter^{-1}$ (Fig. 3D and fig. S12), which are lower than values reported for major OMZs in the eastern Pacific and the Arabian Sea (~11 to 20 μmol N $liter^{-1}$) (*17*, *35*). Combined with water mass residence time, this inventory corresponds to a fixed N loss rate of ~0.4 ± 0.1 mmol m^{-2} day^{-1} (see supplementary materials). These values exceed previous Bay of Bengal estimates based on N^* (2 to 3 μmol N $liter^{-1}$) and N_2/Ar excess (4 to 6 μmol N $liter^{-1}$; Fig. 3D) (*40*), indicating that Δ_{30} resolves a larger biogenic N_2 inventory than conventional nutrient and dissolved-gas proxies. Because Δ_{30} constrains biogenic N_2 accumulation independent of assumed nutrient stoichiometry or background gas corrections, these results suggest that fixed N loss in the sampled Bay of Bengal OMZ waters may be more extensive than previously inferred, while recognizing that temporal variability may also contribute to the discrepancy with earlier N^* and N_2/Ar estimates. Although individual Δ_{30} measurements currently have relatively large analytical uncertainties owing to counting statistics, these can be substantially reduced through longer measurement times and replicate analyses. Future high-precision Δ_{30} transects across major OMZs, ideally

Downloaded from https://www.science.org at University of California Los Angeles on October 08, 2026

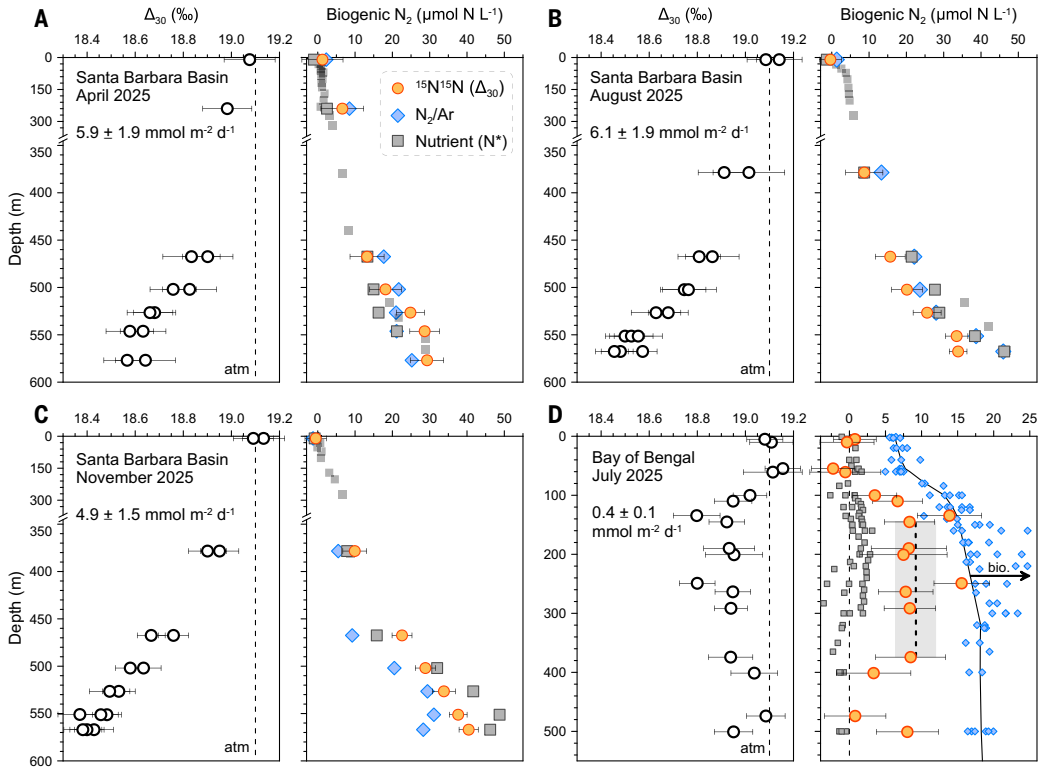


Fig. 3. Comparison of Δ_{30}-, gas-, and nutrient-based proxies of marine nitrogen loss. Depth profiles of Δ_{30} and biogenic N_2 concentrations in Santa Barbara Basin during (**A**) April 2025, (**B**) August 2025, and (**C**) November 2025, and in the Bay of Bengal during (**D**) July 2025. The dashed vertical line marks the atmospheric Δ_{30} value (19.1‰). Biogenic N_2 concentrations derived from Δ_{30} are compared with those inferred from N_2/Ar ratios and nutrient deficits (*N**). Error bars indicate 1 standard error. In (D), the thick dashed line indicates the mean Δ_{30}-derived biogenic N_2 concentration within the OMZ core, and the gray band shows ±1 SD. The areal fixed N loss rates shown in (A) to (C) are snapshot diffusive-flux estimates derived from the vertical gradients in Δ_{30}-derived biogenic N_2, whereas the rate shown in (D) is an inventory-based estimate derived from the biogenic N_2 inventory within the OMZ core and its estimated water mass turnover time. Bay of Bengal N_2/Ar and *N** data are from Bristow *et al*. (*40*). Despite correction for background N_2/Ar, a residual excess N_2 signal remains, indicating incomplete removal of physically enriched N_2 in (D). The solid black line represents a background profile estimated with locally weighted scatterplot smoothing (LOWESS) regression, and deviations from this curve are interpreted as biogenic N_2.

paired with synoptic nutrient and N_2/Ar measurements, could provide direct observational constraints on the magnitude of oceanic fixed N loss.

Identifying sedimentary hotspots of nitrogen loss

Marine sediments associated with methane seeps are localized hotspots of nitrogen loss (*42*). Sulfide-oxidizing bacteria in microbial mats can accumulate nitrate within intracellular vacuoles and couple sulfide oxidation to nitrate reduction, producing either N_2 or ammonium (*43*, *44*). In sediments from methane seeps along the Aleutian Trench, Δ_{30} decreases from 19.1‰ in bottom water to ~16‰ in the porewater of surface sediments (Fig. 4 and fig. S13), indicating substantial accumulation of biogenic N_2 in mat-covered sediments. Sediments without visible microbial mats show much smaller Δ_{30} shifts and lower biogenic N_2 concentrations, confirming that microbial mats drive enhanced fixed N loss at seep sites. These results demonstrate that natural $^{15}N^{15}N$ abundances can identify spatially localized hotspots of microbial N_2 production in sediments, providing a new tool for constraining heterogeneous sedimentary contributions to fixed N loss.

A universal tracer of nitrogen loss across aquatic ecosystems

Across aquifers, lakes, coastal basins, OMZs, and marine sediments, natural $^{15}N^{15}N$ abundances provide a direct tracer of biological N_2 production associated with fixed N loss. Unlike existing proxies, Δ_{30} distinguishes biological N_2 production from physical gas-exchange processes and opposing biological fluxes such as nitrogen fixation. By integrating Δ_{30}-derived biogenic N_2 concentrations with transport modeling, N_2 isotopologue measurements can be converted into areal fixed N loss rates that are directly comparable across environments. Together, these results establish Δ_{30} as a general framework for quantifying fixed N loss across aquatic ecosystems.

The ability to quantify biogenic N_2 without background correction or experimental perturbation is immediately relevant to groundwater remediation, lake eutrophication, and expanding ocean deoxygenation (*45*–*47*). Δ_{30} is particularly powerful in redox-sensitive boundary environments, where fixed N budgets remain poorly constrained (*15*, *29*, *39*, *48*–*50*). Application of Δ_{30} to isolated systems could also be informative. For example, measurements in subglacial Lake Vostok could test whether biogenic N_2 accumulates in a long-isolated, ice-sealed reservoir, with possible relevance to astrobiological exploration of other ice-covered ocean worlds. Because Δ_{30} directly records the molecular origin of N_2, it provides an independent constraint on fixed N loss, complementing and, in key respects, surpassing nutrient-, tracer-, and noble gas–based approaches used in Earth system models.

Improved fixed N loss estimates may have important global implications, as revisions to biogenic N_2 inventories translate into changes in total fixed N loss rates and inferred budget imbalances. As shown above, stoichiometric approaches based on nutrient deficits may either over- or underestimate fixed N loss, depending on how background nutrient stoichiometry is represented. More recent ocean circulation inverse models have improved on simple *N** methods by jointly interpreting nutrient distributions, transport, and variable stoichiometry.

Downloaded from https://www.science.org at University of California Los Angeles on October 08, 2026

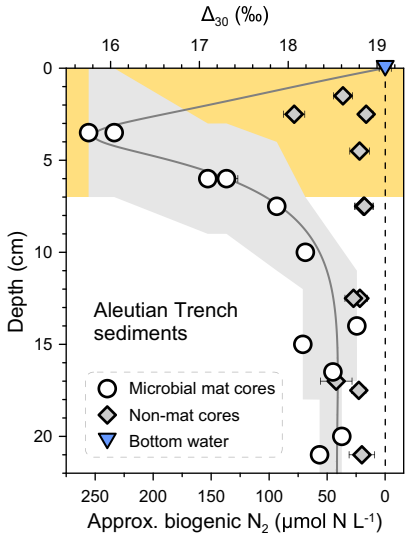


Fig. 4. Nitrogen loss in methane-seep sediments of the Aleutian Trench. Profiles show Δ_{30} with sediment depth. Error bars indicate 1 standard error. The dashed vertical line indicates the bottom-water Δ_{30} value. Yellow shading indicates the depth interval of microbial mat occurrence. Gray shading denotes the vertical range represented by each measurement, reflecting integration of the signal over several centimeters of sediment. The lower axis provides an approximate linearized conversion from Δ_{30} to biogenic N_2; the exact relationship is slightly nonlinear because total dissolved N_2 varies with biogenic N_2 accumulation. The gray curve shows the best-fit reactive transport model to the microbial mat-core Δ_{30} profile. The model is an illustration of how Δ_{30} could constrain rates of sedimentary fixed N loss, given greater depth resolution than that shown here (see supplementary materials).

For example, Wang *et al.* (*13*) inferred ~160 ± 50 Tg N $year^{-1}$ of microbial N_2 fixation, plus ~30 to 40 Tg N $year^{-1}$ of external fixed N inputs, balanced by a total marine fixed N loss of ~200 ± 60 Tg N $year^{-1}$. Yet these global rates remain weakly bounded, particularly for benthic denitrification. Independent constraints such as Δ_{30} could therefore help tighten estimates of total fixed N loss, reveal transient imbalances that are otherwise difficult to detect, and ultimately address one of the central questions in biogeochemistry: whether the global nitrogen cycle is balanced (*3*, *6*, *7*, *13*, *14*). Realizing this potential will require expanded Δ_{30} measurements across the major marine, freshwater, and terrestrial settings of fixed N loss to determine how local estimates of biological N_2 production can be integrated into regional and global nitrogen budgets.

REFERENCES AND NOTES

1. M. M. M. Kuypers, H. K. Marchant, B. Kartal, *Nat. Rev. Microbiol.* **16**, 263–276 (2018).
2. D. E. Canfield, A. N. Glazer, P. G. Falkowski, *Science* **330**, 192–196 (2010).
3. N. Gruber, J. N. Galloway, *Nature* **451**, 293–296 (2008).
4. S. Seitzinger *et al.*, *Ecol. Appl.* **16**, 2064–2090 (2006).
5. X. Zhang, B. B. Ward, D. M. Sigman, *Chem. Rev.* **120**, 5308–5351 (2020).
6. L. A. Codispoti *et al.*, *Sci. Mar.* **65**, 85–105 (2001).
7. C. Deutsch, J. L. Sarmiento, D. M. Sigman, N. Gruber, J. P. Dunne, *Nature* **445**, 163–167 (2007).
8. P. M. Groffman *et al.*, *Ecol. Appl.* **16**, 2091–2122 (2006).
9. M. Feng *et al.*, *Nat. Commun.* **14**, 3065 (2023).
10. N. Gruber, J. L. Sarmiento, *Global Biogeochem. Cycles* **11**, 235–266 (1997).
11. T. DeVries, C. Deutsch, F. Primeau, B. Chang, A. Devol, *Nat. Geosci.* **5**, 547–550 (2012).
12. L. P. Nielsen, *FEMS Microbiol. Lett.* **86**, 357–362 (1992).
13. W.-L. Wang, J. K. Moore, A. C. Martiny, F. W. Primeau, *Nature* **566**, 205–211 (2019).
14. C. Deutsch, T. Weber, *Annu. Rev. Mar. Sci.* **4**, 113–141 (2012).
15. M. J. Ascott *et al.*, *Nat. Commun.* **8**, 1416 (2017).
16. S. Emerson, S. Bushinsky, *J. Geophys. Res. Oceans* **121**, 4360–4376 (2016).
17. B. X. Chang, A. H. Devol, S. R. Emerson, *Global Biogeochem. Cycles* **26**, GB3030 (2012).
18. A. M. Seltzer *et al.*, *Proc. Natl. Acad. Sci. U.S.A.* **120**, e2217946120 (2023).
19. L. Y. Yeung *et al.*, *Sci. Adv.* **3**, eaao6741 (2017).
20. L. Y. Yeung *et al.*, *Environ. Sci. Technol.* **53**, 5168–5175 (2019).
21. H. Yan, F. Tong, Y. Peng, Y. Shang, H. Bao, *Anal. Chem.* **97**, 24317–24325 (2025).
22. J. C. Vogel, A. S. Talma, T. H. E. Heaton, *J. Hydrol.* **50**, 191–200 (1981).
23. J. K. Böhlke, R. Wanty, M. Tuttle, G. Delin, M. Landon, *Water Resour. Res.* **38**, 1105 (2002).
24. T. H. E. Heaton, J. C. Vogel, *J. Hydrol.* **50**, 201–216 (1981).
25. W. Aeschbach-Hertig, F. Peeters, U. Beyerle, R. Kipfer, *Nature* **405**, 1040–1044 (2000).
26. A. L. Popp, C. C. Manning, M. S. Brennwald, R. Kipfer, *Environ. Sci. Technol.* **54**, 1562–1572 (2020).
27. W. Aeschbach-Hertig, H. El-Gamal, M. Wieser, L. Palcsu, *Water Resour. Res.* **44**, W08449 (2008).
28. H. Craig, R. A. Wharton Jr., C. P. McKay, *Science* **255**, 318–321 (1992).
29. B. M. Loeks, J. B. Cotner, *Proc. Natl. Acad. Sci. U.S.A.* **117**, 17063–17067 (2020).
30. R. Kipfer, W. Aeschbach-Hertig, F. Peeters, M. Stute, *Rev. Mineral. Geochem.* **47**, 615–700 (2002).
31. Z. Stevenson *et al.*, *Commun. Earth Environ.* **7**, 169 (2026).
32. S. J. Bograd, F. B. Schwing, C. G. Castro, D. A. Timothy, *J. Geophys. Res.* **107**, 3216 (2002).
33. A. Bourbonnais, M. F. Lehmann, R. C. Hamme, C. C. Manning, S. K. Juniper, *Mar. Chem.* **157**, 194–207 (2013).
34. D. L. Valentine *et al.*, *Environ. Sci. Technol.* **50**, 11057–11065 (2016).
35. B. X. Chang, A. H. Devol, S. R. Emerson, *Deep Sea Res. Part I Oceanogr. Res. Pap.* **57**, 1092–1101 (2010).
36. W. M. Berelson, D. E. Hammond, C. Fuller, *Earth Planet. Sci. Lett.* **61**, 41–54 (1982).
37. D. M. Sigman *et al.*, *Geochem. Geophys. Geosyst.* **4**, 1040 (2003).
38. N. Risgaard-Petersen, L. P. Nielsen, S. Rysgaard, T. Dalsgaard, R. L. Meyer, *Limnol. Oceanogr. Methods* **1**, 63–73 (2003).
39. A. Paulmier, D. Ruiz-Pino, *Prog. Oceanogr.* **80**, 113–128 (2009).
40. L. A. Bristow *et al.*, *Nat. Geosci.* **10**, 24–29 (2017).
41. E. A. Howell, S. C. Doney, R. A. Fine, D. B. Olson, *Geophys. Res. Lett.* **24**, 2549–2552 (1997).
42. Q. Jiang *et al.*, *Nat. Commun.* **16**, 1646 (2025).
43. H. Fossing *et al.*, *Nature* **374**, 713–715 (1995).
44. C. A. Schutte *et al.*, *Appl. Environ. Microbiol.* **84**, e02860-17 (2018).
45. M. O. Rivett, S. R. Buss, P. Morgan, J. W. N. Smith, C. D. Bemment, *Water Res.* **42**, 4215–4232 (2008).
46. R. F. Keeling, A. Körtzinger, N. Gruber, *Annu. Rev. Mar. Sci.* **2**, 199–229 (2010).
47. D. W. Schindler *et al.*, *Proc. Natl. Acad. Sci. U.S.A.* **105**, 11254–11258 (2008).
48. A. J. Burgin, S. K. Hamilton, *Front. Ecol. Environ.* **5**, 89–96 (2007).
49. S. P. Seitzinger, *Limnol. Oceanogr.* **33**, 702–724 (1988).
50. P. J. Mulholland *et al.*, *Nature* **452**, 202–205 (2008).

ACKNOWLEDGMENTS

We acknowledge the crews and shipboard scientists aboard the research vessels *Atlantis*, *Thomas G. Thompson*, *Yellowfin*, and *Connell*, as well as the HOV *Alvin* team, the CalCOFI team, and Ultima Antarctic Logistics. We gratefully thank R. Hamme, I. Moede, K. Anderson, C. Benitez-Nelson, G. Castle, K. Doyle-Jacobson, L. Guibourdenche, T. Gunderson, E. Halewood, K. Homola, E. Klonicki-Ference, L. Levin, K. Lloyd, C. Manning, K. Marchus, S. Martinez, A. Martiny, M. Packebush, X. Peng, C. Pierre, J. Pritzker, A. Santoro, R. Swalethorp, R. Thomason, L. Trottier, G. Vetushko, E. Wessenauer, L. Wharram, C. Yoder, and B. B. Jørgensen for field assistance, equipment support, or helpful discussions. **Funding:** This work was supported by Simons Postdoctoral Fellowship SFI-LS-FMME-00008334 from the Simons Foundation International (J.L.), NASA grant 80NSSC21K0477 (E.D.Y.), NASA grant NNX16AB69A (D.T.A.), NASA grant 80NSSC19K0474 (E.D.S.), NASA Postdoctoral Fellowship at the UCR Astrobiology Center (A.J.), NSF grant EAR-2238641 (A.M.S.), NSF grant EAR-1944946 (E.D.S.), NSF grant OCE-2319096 (A.B.), NSF grant OCE-1830033 (D.L.V.), NSF grant OCE-2048597 (T.T.), NSF grant OCE-2048666 (V.J.O.), Natural Sciences and Engineering Research Council of Canada grant RGPIN-2022-04305 (A.P.), the Tawani Foundation (D.T.A.), the Trottier Family Foundation (D.T.A.), the New Frontiers Research Fund – Exploration (D.L.), the Geology Foundation at the University of Texas at Austin (M.B.C.), and University of Basel Strategic Project Funding (M.F.L.). **Author contributions:** Conceptualization: J.L., E.D.Y., D.L.V., A.M.S., A.B., A.P., E.D.S.; Funding acquisition: J.L., E.D.Y., D.L.V., A.M.S., A.B., A.P., E.D.S., T.T., M.B.C., M.F.L., V.J.O., D.T.A., D.L., A.J.; Investigation: J.L., E.D.Y., D.L.V., A.B., D.T.A., D.B., G.B., M.B.C., D.F., C.F., K.M.G., A.J., F.S.K., D.L., M.F.L., K.M., J.M., V.J.O., A.P., E.R., E.D.S., T.T., A.M.S.; Supervision: E.D.Y., D.L.V., A.M.S.; Writing – original draft: J.L.; Writing – review & editing: J.L., E.D.Y., D.L.V., A.B., D.T.A., D.B., G.B., M.B.C., D.F., C.F., K.M.G., A.J., F.S.K., D.L., M.F.L., K.M., J.M., V.J.O., A.P., E.R., E.D.S., T.T., A.M.S. **Competing interests:** The authors declare that they have no competing interests. **Data, code, and materials availability:** All data are available in the main text or the supplementary materials. No new materials were generated for this study.

License information: Copyright © 2026 the authors, some rights reserved; exclusive licensee American Association for the Advancement of Science. No claim to original US government works. https://www.science.org/about/science-licenses-journal-article-reuse

SUPPLEMENTARY MATERIALS

science.org/doi/10.1126/science.aei0940
Materials and Methods; Figs. S1 to S17; References (*51*–*105*); Data S1

Submitted 16 April 2026; accepted 13 August 2026

10.1126/science.aei0940

Downloaded from https://www.science.org at University of California Los Angeles on October 08, 2026

Science
AAAS

Natural $^{15}N^{15}N$ abundances constrain fixed nitrogen loss

Jiarui Liu, David L. Valentine, Annie Bourbonnais, Dale T. Andersen, Daniele Bianchi, Grace Brown, M. Bayani Cardenas, Daniel Fillion, Claudia Frey, Kelsey M. Gosselin, Aoshuang Ji, Franklin S. Kinnaman, Denis Lacelle, Moritz F. Lehmann, Katelyn McPaul, James Mullahoo, Victoria J. Orphan, André Pellerin, Elen Reji, Elizabeth D. Swanner, Tina Treude, Alan M. Seltzer, and Edward D. Young

Science **394** (6820), . DOI: 10.1126/science.aei0940

Editor's summary

Nitrogen gas (N_2) is produced naturally by either photochemical reactions in the atmosphere or microbial processes in the biosphere, but the magnitudes of those sources are poorly quantified. Liu *et al*. showed that the abundance of the rare $^{15}N^{15}N$ isotopologue can be used to determine the amount of biogenic N_2 production in aquatic environments, thereby allowing physical and biological N_2 sources to be distinguished. This approach, applied to a wide spectrum of surface and ground water bodies, will help to better constrain the global nitrogen cycle. —Jesse Smith

View the article online
https://www.science.org/doi/10.1126/science.aei0940
Permissions
https://www.science.org/help/reprints-and-permissions

Downloaded from https://www.science.org at University of California Los Angeles on October 08, 2026

Use of this article is subject to the Terms of service

Science (ISSN 1095-9203) is published by the American Association for the Advancement of Science. 1200 New York Avenue NW, Washington, DC 20005. The title *Science* is a registered trademark of AAAS.

Copyright © 2026 The Authors, some rights reserved; exclusive licensee American Association for the Advancement of Science. No claim to original U.S. Government Works